Biochimica et Biophysica Acta 1818 (2012) 2732–2741

Contents lists available at SciVerse ScienceDirect

Biochimica et Biophysica Acta

journal homepage: www.elsevier.com/locate/bbamem

Difference in lipid packing sensitivity of exchangeable apolipoproteins apoA-I and apoA-II: An important determinant for their distinctive role in lipid metabolism

Lionel Chièze [b], Victor Martin Bolanos-Garcia [a], Gérard Le Caër [b], Anne Renault [b], Véronique Vié [b,*], Sylvie Beaufils [b,*]

[a] Department of Biochemistry, University of Cambridge, Cambridge CB2 1GA, UK
[b] Institut de Physique de Rennes, UMR-CNRS 6251 Université de Rennes 1, Campus de Beaulieu, Rennes cedex, France

ARTICLE INFO

Article history:
Received 14 December 2011
Received in revised form 11 May 2012
Accepted 14 May 2012
Available online 22 May 2012

Keywords:
Exchangeable apolipoprotein
Lipid packing sensitivity
Phospholipid monolayer
AFM measurement
Statistical analysis of planar point process

ABSTRACT

Exchangeable apolipoproteins A-I and A-II play distinct roles in reverse cholesterol transport. ApoA-I interacts with phospholipids and cholesterol of the cell membrane to make high density lipoprotein particles whereas apolipoprotein A-II interacts with high density lipoprotein particles to release apolipoprotein A-I. The two proteins show a high activity at the aqueous solution/lipid interface and are characterized by a high content of amphipathic α-helices built upon repetition of the same structural motif. We set out to investigate to what extent the number of α-helix repeats of this structural motif modulates the affinity of the protein for lipids and the sensitivity to lipid packing. To this aim we have compared the insertion of apolipoproteins A-I and A-II in phospholipid monolayers formed on a Langmuir trough in conditions where lipid packing, surface pressure and charge were controlled. We also used atomic force microscopy to obtain high resolution topographic images of the surface at a resolution of several nanometers and performed statistical image analysis to calculate the spatial distribution and geometrical shape of apolipoproteins A-I and A-II clusters. Our data indicate that apolipoprotein A-I is sensitive to packing of zwitterionic lipids but insensitive to the packing of negatively charged lipids. Interestingly, apolipoprotein A-II proved to be insensitive to the packing of zwitterionic lipids. The different sensitivity to lipid packing provides clues as to why apolipoprotein A-II barely forms nascent high density lipoprotein particles while apolipoprotein A-I promotes their formation. We conclude that the different interfacial behaviors of apolipoprotein A-I and apolipoprotein A-II in lipidic monolayers are important determinants of their distinctive roles in lipid metabolism.

1. Introduction

ApoA-I and apoA-II are two major constituents of HDL particles and are implicated in reverse cholesterol transport (RCT), a process that is central to lipid metabolism in higher organisms. ApoA-I and apoA-II belong to the family of exchangeable apolipoproteins and despite the low amino acid sequence homology and different size, both are largely organized as amphipathic α-helix tandem repeats [1]. The number of such α-helix repeats confer these proteins a high affinity for hydrophobic–hydrophilic interfaces [2–6]. In consequence, both apoA-I and apoA-II have the ability to recruit phospholipids from the cell surface to form pre-HDL particles [7–11] but apoA-I is more efficient in creating pre-HDL particles than apoA-II. Indeed, the proportion of lipoproteins containing apoA-II is less than 10% of the total amount of HDL [12,13]. Taken together, these data indicate that apoA-I plays a central role in RCT and exerts a cardioprotective effect while apoA-II acts as a regulatory factor on RCT, as suggested by Scanu in a recent review [14]. Hence, these proteins have different biological functions although they both contain amphipathic α-helices.

Vedhachalam et al. proposed a model for the formation of high density lipoproteins by apoA-I, where apoA-I is preferentially inserted into protrusions at the cell membrane and forms lipoproteins from these regions [11]. In this model, the formation of these protrusions is driven by the ATP-binding cassette transporter A1 (ABCA1) following apoA-I activation [9,15,16]. ABCA1 causes an excess of lipid in the external leaflet by translocation of lipids from the internal leaflet of the plasma membrane [9,16]. The occurrence of protrusions lowers the lipid packing in the external leaflet of the membrane and permits the binding of apoA-I at the membrane into the protrusions. Others have shown that the efficiency of apoA-I mimetic peptides in promoting the efflux of cholesterol increases with the number of α-helix repeats [17–19]. Therefore, lipid packing and

Abbreviations: AFM, atomic force microscopy; ALPS, amphipathic lipid packing sensor; apoA-I, apolipoprotein A-I; CE, esterified cholesterol; DPPC, dipalmitoyl-phosphatidylcholine; DPPG, dipalmitoyl-phosphatidylglycerol; DOPC, dioleoyl-phosphatidylcholine; HDL, high density lipoprotein; LE, liquid-expanded; LC, liquid-condensed; LCAT, lecithin: cholesterol acyltransferase; RCT, reverse cholesterol transport

* Corresponding authors at: IPR UMR 6251, Université de Rennes 1. Bat 11A, Campus Beaulieu, 35042, Rennes cedex, France. Tel.: +33 0223235700; fax: +33 0223236717.
E-mail addresses: veronique.vie@univ-rennes1.fr (V. Vié), sylvie.beaufils@univ-rennes1.fr (S. Beaufils).

0005-2736/$ – see front matter © 2012 Elsevier B.V. All rights reserved.
doi:10.1016/j.bbamem.2012.05.016

the number of α-helix repeats in the protein structure seem to be important factors for the role of apoA-I in HDL formation.

In a recent study, we have shown that apoA-I is sensitive to the packing of zwitterionic lipids and lipid compressibility when interacting with a model membrane [10]. Importantly, the sensitivity of apoA-I to lipid packing was not observed in anionic lipids. We hypothesized that the interaction of residues defining the hydrophobic face of the amphipathic α-helix tandem repeats with lipid chains confers apoA-I and apoA-II a distinctive lipid packing sensitivity. We also hypothesized that in such scenario the insertion of exchangeable apolipoproteins into the external protrusions is less favored for long amphipathic α-helix tandem repeat motifs compared to shorter ones and that this in turn confers apoA-I and apoA-II a different lipid packing sensitivity.

To test these hypotheses we used a Langmuir trough to mimic a biological system. In this set up the proteins are injected below lipidic monolayers at a concentration that favors protein–lipid interactions. Lipids are spread at the buffer surface and compressed with movable barriers thus allowing a tight control of the molecular area per lipid (i.e., lipid packing) in the trough. High resolution topographic images of the surface were obtained by transferring the interfacial layer on mica sheets and the subsequent observation by atomic force microscopy (AFM) at a resolution of several nanometers [20,21]. A series of statistical image analyses [10,22] of each AFM image was performed to calculate the spatial repartition of apoA-I clusters inserted in zwitterionic phospholipid [dipalmitoyl-phosphatidyl-choline (DPPC), dioleoyl-phosphatidylcholine (DOPC)] and anionic phospholipid [dipalmitoyl-phosphatidyl-glycerol (DPPG)] monolayers. We compared these results with the spatial repartition of apoA-II in zwitterionic phospholipids and the geometrical shape of apoA-II and apoA-I clusters inserted in zwitterionic DPPC.

Our analyses suggest that a high fraction of apoA-I in phospholipid monolayers is present as small oligomers that in principle can promote HDL formation. Although apoA-II was far less sensitive to lipid packing, it is inserted in the lipidic layer as clusters of similar self-assembly constant as apoA-I clusters. The difference in lipid packing sensitivity explains why apoA-II forms very few nascent HDL particles while apoA-I promotes their formation. The observed dissimilarity in the interfacial behavior of these two proteins in the lipidic layer provides new insights into the molecular features that are important for their distinctive biological functions.

2. Materials and methods

2.1. Protein expression and purification

Recombinant apolipoproteins were cloned into a pET expression vector and expressed in *Escherichia coli* Rosetta 2 cells at 37 °C, 250 rpm in 2xTY broth. When cell density of 0.6–0.8 at OD600 nm was reached, cells were induced with IPTG. Inclusion bodies were resuspended in denaturing buffer (i.e., 10 mM Tris buffer containing 8 M urea, 25 mM imidazole, and 5 mM beta-mercaptoethanol, pH 8.0). The resulting solution was loaded onto one chromatographic column packed with Ni-NTA agarose previously equilibrated in the same buffer solution. After being washed with at least 20 column volumes, recombinant apolipoproteins were refolded by quick dilution in TBS buffer containing 1 M arginine, and concentrated using vivaspin centrifuge tubes. Refolded apolipoproteins were subjected to thrombin cleavage after extensive dialysis in TBS. One unit of thrombin protease of high purity was used to digest 1 mg of recombinant apolipoproteins for 6–8 h at 4 °C. Thrombin and the cleaved histidine tag were removed using a benzamidine fast flow column and a Ni-NTA column, respectively, previously equilibrated in TBS. As the final purification step, apolipoproteins were loaded onto a gel filtration column (Superdex 75, HR 26/60), and eluted in 20 mM Tris buffer, 200 mM NaCl, pH 8.0 (TBS buffer) at 1 ml/min. After analysis by SDS-PAGE and measurement of UV absorption spectra (200–300 nm), fractions containing pure apolipoproteins were collected and concentrated. Pure recombinant apolipoproteins were concentrated five-fold and stored at −20 °C. N-terminal sequence and mass spectrometry were carried out to confirm protein identity and purity of recombinant apolipoproteins.

2.2. Circular dichroism

To confirm that apolipoproteins were refolded to the native state, far-UV circular dichroism spectra were recorded on an AVIV 62-S spectropolarimeter (AVIV, Lakewood, NJ) previously calibrated with camphorosulfonic acid and equipped with a temperature control unit. In all experiments, spectra were recorded at 20 °C in a 0.1 cm quartz cell using an average time of 0.5 s, a step size of 0.5 nm, and a 1 nm bandwidth and averaged over 20 scans. Independently prepared protein samples of concentrations ranging between 40 and 400 μg/ml were used. After subtraction of the buffer baseline, the CD data were normalized and reported as molar residue ellipticity. The concentration of protein solutions was determined from amino acid composition analysis at the PNAC facility (Department of Biochemistry, University of Cambridge). Far-UV CD analysis of all proteins was carried out immediately after gel filtration chromatography, as shown in the Supplementary material.

2.3. Buffer and protein concentration

Experiments with apoA-I were performed at 1.5 μg/ml in 20 mM phosphate buffer solution which was prepared from 20 mM Na_2HPO_4 and 20 mM NaH_2PO_4 stock solutions mixed to give a final solution of pH = 7.0 and temperature of 20 ± 2 °C. The concentration of monomeric apoA-I was 53.10^{-9} M.

For apoA-I sub-phase concentrations superior to 3.0 μg/ml, the surface pressure value was 22 mN/m. In this condition, the liquid/air interface was saturated with the protein thus allowing potential protein–protein interactions in the subphase. At the experimental subphase apoA-I concentration of 1.5 μg/ml, the surface pressure was lower (17 mN/m) and the protein molecules did not saturate the liquid/air interface. Hence, at the aqueous solution/lipid interface and with 1.5 μg/ml of apoA-I in the subphase, it is reasonable to assume that apoA-I–lipid interactions are favored over protein–protein interactions [23].

Experiments with apoA-II were performed at 0.8 μg/ml in the same phosphate buffer and temperature as apoA-I. The concentration of apoA-II dimers was estimated to be equal to the concentration of apoA-I monomers (53.10^{-9} M).

2.4. Phospholipids

Three phospholipids were chosen to distinguish phase effect from charge effect: the zwitterionic lipids DPPC and DOPC, and the anionic lipid DPPG. DPPC and DPPG have saturated acyl chains and show first order phase transition from expanded liquid phase LE to condensed liquid phase LC [24,25]. DOPC has unsaturated acyl chains and is always in LE phase [25].

The three phospholipids were purchased from Avanti Polar Lipids (Alabama, U.S.). Solutions at 0.5 mM of DPPC, DOPC and DPPG were prepared by dissolving the phospholipids in chloroform. Before each experiment, an isotherm was performed on the phospholipid stock solution in order to assess lipid stability.

2.5. Monolayer and Langmuir–Blodgett techniques

Experiments were performed with a computer-controlled and user-programmable Langmuir Teflon-coated trough (type 601BAM, equipped with two movable barriers with total surface of 716 cm^2,

Nima Technology Ltd., England). Before starting experiments, the trough was cleaned successively with ultrapure water (Nanopure-UV), ethanol and finally warm ultrapure water.

The trough was filled with 20 mM phosphate buffer at pH 7 and a temperature of 20 ± 2 °C. Phospholipids were spread over the clean liquid/air interface between movable barriers using a high precision Hamilton microsyringe. After phospholipid spreading, no surface pressure was detectable. After 10 min to allow evaporation of the solvent, films were compressed by the moving barriers at a rate of 20 cm^2/min up to the required surface pressure (π_i). The barriers were then maintained at a fixed position (so that the surface of the trough was kept constant) and the proteins were injected into the subphase with a syringe. The needle of the syringe passed under a barrier and in this case the phospholipid monolayer was not perturbed.

Surface pressure was measured according to the Wilhelmy-plate method using a filter paper connected to a microelectronic feedback system for surface pressure measurements. Values of surface pressure (π) were stable and recorded every 4 s with a precision of ± 0.2 mN/m.

For imaging pure monolayers of phospholipids (without injection of proteins), the film was transferred to a mica support previously immersed in the subphase following the Langmuir–Blodgett method. The transfer speed was 0.16 mm/min. In the case of protein injection, the mixed monolayer was transferred at the equilibration state (i.e. surface pressure attained a plateau) to a mica support that was not previously immersed in the subphase unlike the case of phospholipid monolayers. The transfer speed was kept constant at 0.16 mm/min. Pure phospholipid monolayers and mixed monolayers of proteins/phospholipids were transferred to freshly-cleaved mica surfaces.

2.6. AFM measurements

Surface images of the Langmuir–Blodgett monolayers were recorded with a Pico-plus atomic force microscope (Molecular Imaging, Phoenix, AZ) operating in contact mode. Two scanners of 100 μm and 10 μm were used for measurements. Topographic images were acquired in constant force mode using silicone nitride tips with nominal spring constant of 60 mN/m.

AFM images of 64 μm^2 size, with lateral resolution of ~250 nm^2 by pixel were analyzed to characterize the geometry of protein clusters. For these images the resolution of the height is 0.117 nm (Z-range = 30 nm; 256 levels of gray). These images were exported from the AFM microscope in TIFF format. The images were analyzed with the public image processing program ImageJ (http://rsbweb.nih.gov/ij/). To measure the position of protein cluster centers in apoA-I/phospholipids and apoA-II/phospholipids monolayers, we used a home-made program [10,22] running with ImageJ. This program gives the position of protein cluster centers only if these protein clusters are higher than a threshold height. Then, we adjusted the threshold height to measure the maximum elevation of protein clusters. However, the threshold height must be sufficiently high to prevent the selection of lipid areas. In the case of DPPC, objects formed in the LE phase of DPPC have sometimes the same height as LC lipid domains. In order to prevent the possibility to get LC lipid domains in our analysis we eliminated all objects of this height.

The same home-made program permits the determination of surface and height of protein clusters from AFM images. Then, we built histograms of the height and surface of protein clusters and plot protein cluster height as a function of protein cluster surface. The histograms were normalized by the total number of clusters used for histogram building (Table 1). The histograms thus represent the probability of protein clusters to adopt a particular height or surface.

Table 1
Total numbers of AFM images and protein clusters used for statistical analyses.

	Number of AFM images (number of clusters)
A-I/DOPC	6 (2065)
A-I/DPPC	6 (328)
A-I/DPPG	8 (1351)
A-I/DOPC Gray level 149	6 (1156)
A-II/DPPC	14 (3785)

2.7. Analysis of the distribution of protein clusters on the AFM images

Because the distribution of protein clusters recorded by AFM provides insights into cluster–cluster interactions, the distribution functions: D(r), V(r) and g(r) were calculated from cluster centers of each AFM image.

- D(r) is the probability to find a distance equal to or less than r from one cluster to its nearest-neighbor cluster. This distribution function can reveal the presence of short-range interactions between clusters and the type of these interactions (attractive or repulsive).
- V(r) is the probability to find a distance less than r or equal to from a randomly-distributed point to the nearest cluster. This function is very sensitive to the distribution of empty spaces between the clusters and can reveal the presence of long-range interactions between them.
- g(r) is the pair correlation function and represents the variation of the local density compared to the mean density.

Hence, the distribution functions estimated for each AFM image and named $D(r)_{Exp}$, $V(r)_{Exp}$, and $g(r)_{Exp}$ are referred to as "experimental distribution functions" and were compared to two classes of distribution functions:

i. a random distribution of points (also known as a Poisson process), in which the density of points is equal to the mean density of clusters extracted from the AFM image. In this case, points do not interact at all. The functions of this distribution will be referred hereafter as "Poisson distribution functions" and named $D(r)_P$, $V(r)_P$ and $g(r)_P$.
ii. Monte-Carlo simulated distributions of hard-disks, with a number of disks that is the same as the number of clusters on the corresponding AFM image. The functions of these distributions are referred to as "hard-disk distribution functions" and named $D(r)_H$, $V(r)_H$ and $g(r)_H$. The surface of each disk is generated by a Monte-Carlo process. Fig. 6 shows the fit of the cluster diameter distribution to an exponential function for an apoA-I/DOPC monolayer. The diameter distribution of the three apoA-I/phospholipid monolayers was used to simulate the diameter d and the associated surface $(\pi \cdot d^2)/4$ of each disk by the Monte-Carlo method. The same strategy was used for hard-disk simulations of apoA-II/DPPC monolayers.

Detailed information about D(r), V(r) and g(r) estimations are described in the Supplementary material.

3. Results

3.1. ApoA-I clusters are randomly distributed in a LE single-phase monolayer of phospholipids

First, we set out to define apoA-I cluster distribution at $\pi_{initial}$ value of 15 mN/m in a homogeneous single phase monolayer that mimics a low packing region of biological membrane with a surface pressure for which the number of protein clusters allows a statistical analysis. The increase of surface pressure produced by the presence of

apoA-I at the liquid–DOPC interface is 4 mN/m. Hence, the surface pressure during transference on mica sheet is equal to 19 mN/m. We observed that DOPC is in a single (LE) phase (Fig. 1A), while DPPC and DPPG show LE/LC phase coexistence. The AFM image of the apoA-I/DOPC monolayer shown in Fig. 1A allowed the estimation of the experimental distribution functions of apoA-I clusters. We compared it to the hard-disk and the Poisson distribution functions (Fig. 2, panel 1) with an object density that is similar to the cluster density of AFM images. Reproducibility was confirmed with three other DOPC AFM images (data not shown).

For D(r), a similar overall shape for experimental, hard-disk and Poisson curves were observed. However, $D(r)_{Exp}$ is lower than $D(r)_H$ and $D(r)_P$ for distances between centers shorter than 300 nm. The good agreement between $V(r)_{Exp}$, $V(r)_H$ and $V(r)_P$ and between $g(r)_{Exp}$, $g(r)_H$ and $g(r)_P$ strongly suggests that the positions of clusters are weakly correlated for any distance between clusters.

In summary, these estimations evidence weak or non-existent interactions between clusters thus resulting in a random distribution of apoA-I clusters.

3.2. The random distribution of apoA-I clusters in LE phase is not affected by their confinement in LE domains of DPPC

We then investigated apoA-I cluster distribution in a DPPC monolayer a lipid that has the same polar headgroup as in DOPC and showing LE/LC phase coexistence so that the lipid packing of the layer is different to that of LE phase of pure DOPC. The increase of surface pressure produced by the presence of apoA-I at the liquid–DPPC interface is 4 mN/m. Hence, the surface pressure during transference on mica sheet is equal to 19 mN/m. The different acyl chain exerts an important influence on the behavior of these lipids at the interface. For instance, in a previous study [10], we showed that apoA-I is mainly inserted in the LE phase of DPPC monolayers and that the amount of apoA-I in the LC phase was very low compared to the amount of apoA-I in the LE phase of this lipid. This feature evidences that apoA-I cluster distribution is affected by the presence of LE/LC phase coexistence, which prompted us to investigate in more detail the influence of the confinement of apoA-I clusters in LE phase on their distribution function.

AFM images of apoA-I/DPPC (Fig. 1B) showed wide bright gray domains that represented the LC phase and wide dark gray domains representing the LE phase. Fig. 2 (panel 2) shows the protein cluster distribution functions in the phase coexistence that were derived from the AFM-image of DPPC shown in Fig. 1B. Fig. 2 compares the experimental distribution functions of hard disks distributed over the whole surface of the image. Reproducibility was confirmed after recording three independent AFM images of the apoA-I /DPPC monolayers (data not shown). The experimental distribution functions and the random hard-disk distribution functions differ significantly. Indeed, $D(r)_{Exp}$ increases more rapidly with r than $D(r)_H$, $V(r)_{Exp}$ increases less rapidly with r than $V(r)_H$ and $g(r)_{Exp}$ is much larger than $g(r)_H$ for distances less than 1600 nm. The three parameters consistently show that clusters are closer to their first neighbors and that empty spaces are larger than that expected for a random distribution of clusters.

We then studied the distribution of apoA-I clusters into LE domains of DPPC to determine if interactions between clusters are favored by their confinement in the LE phase. The distribution functions were estimated from the positions of apoA-I cluster centers into LE domains of DPPC, without taking into account the clusters in the LC phase. These distribution functions will be referred to as experimental-LE distribution functions. For comparison, we simulated the distribution of clusters in the LE domains of DPPC assuming a random distribution of points and a random distribution of hard-disks. In both cases, the objects were distributed into broad circular domains that have the same centers and areas as LE domains of AFM-images of DPPC. The number of hard-disks and the number of points are equal to the number of protein clusters in LE domains determined from the corresponding AFM image. The distribution functions of hard-disks are referred to here as “hard-disks-LE distribution functions” and named $D(r)_{H\text{-}LE}$, $V(r)_{H\text{-}LE}$ and $g(r)_{H\text{-}LE}$. The distribution

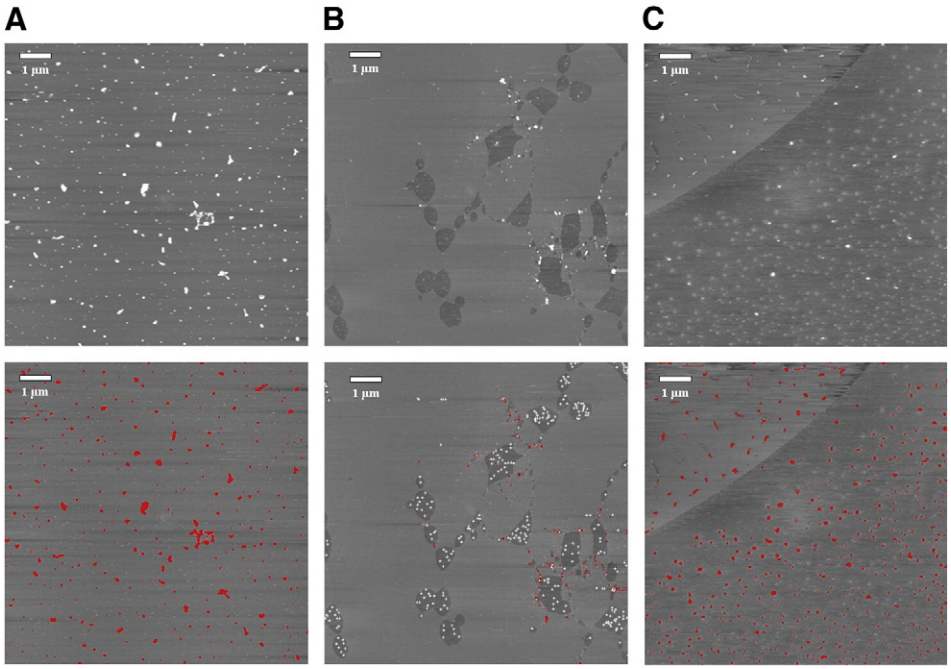

Fig. 1. On the top, AFM images of mixed monolayers of apoA-I/phospholipids, where initial surface pressure was kept at 15 mN/m (size: 64 μm^2 and z-range = 10 nm): DOPC with apoA-I (A), DPPC with apoA-I (B) and DPPG with apoA-I (C). On the bottom, threshold images. For DPPC, the striking difference between the number of clusters in LE phase (marked by white crosses) and the number of clusters in LC phase (colored in red) reveals the difference of apoA-I affinity between LE and LC phase. For DOPC and DPPG, clusters are colored in red for both phases.

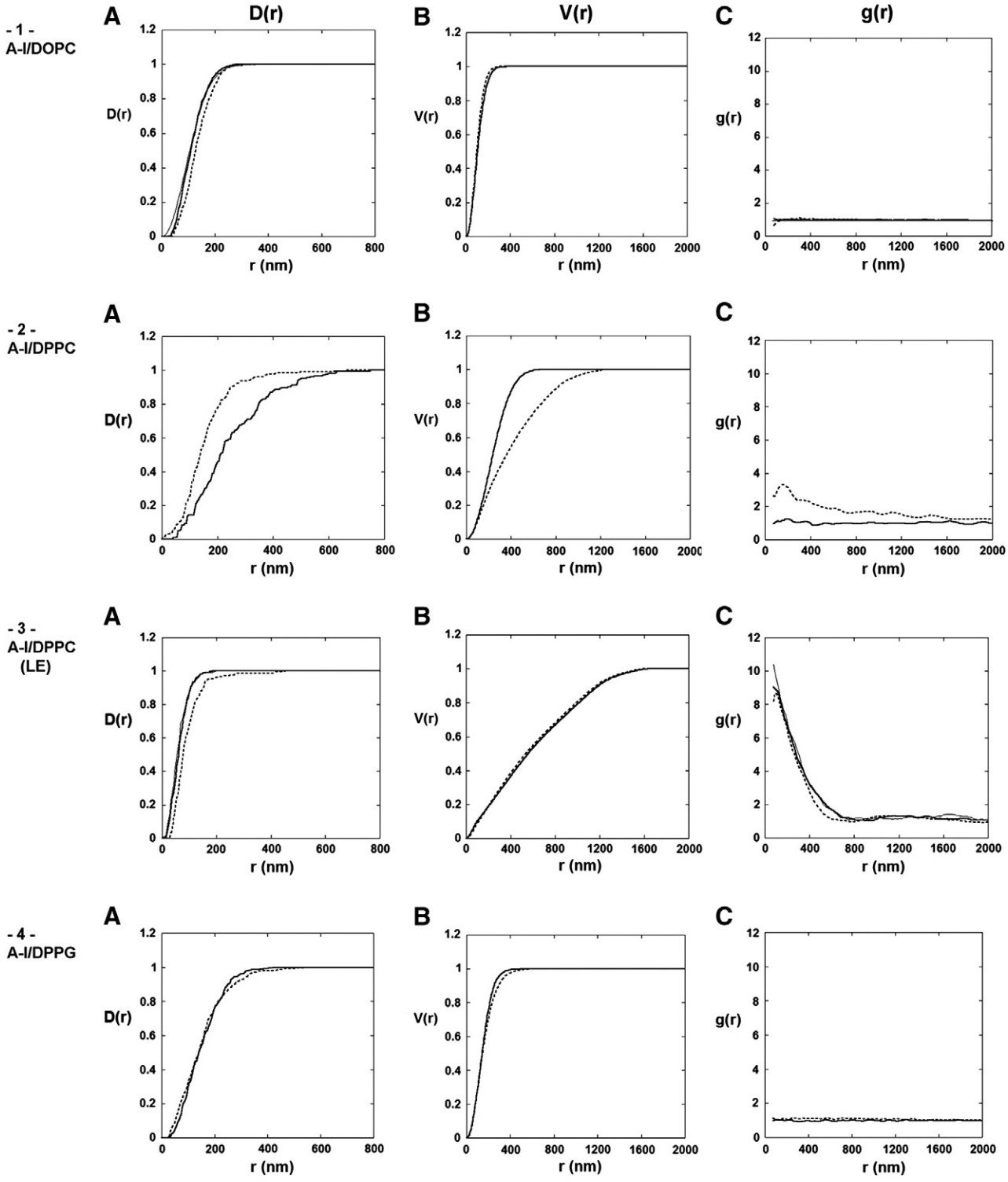

Fig. 2. Analysis of the distribution of protein clusters on AFM-images of apoA-I/phospholipids (starting surface pressure 15 mN/m) shown in Fig. 1. Phospholipids are DOPC (panel 1), DPPC (panel 2), LE domains of DPPC (panel 3) and DPPG (panel 4). For each case, D(r) (panel A), V(r) (panel B) and g(r) (panel C) were calculated. The dotted lines show experimental distribution functions of protein clusters; the thick lines show hard-disk distribution functions and the thin lines show the Poisson distribution functions of of panel 1 and 3 (for panel 3, see paragraph 3.2 for details).

functions for points (null surface) will be referred to as "Poisson-LE distribution functions" and named $D(r)_{P\text{-}LE}$, $V(r)_{P\text{-}LE}$ and $g(r)_{P\text{-}LE}$. Fig. 2 (panel 3) shows the distribution functions for the AFM-image of DPPC shown in Fig. 1B. Tests of reproducibility were performed with three other AFM images of DPPC. Experimental-LE, hard-disks-LE and Poisson-LE distribution functions are similar which shows that apoA-I clusters are randomly distributed in the LE phase of DPPC and that interactions do not appear when apoA-I clusters are confined into micrometer sized LE domains.

3.3. ApoA-I cluster distribution in anionic lipids

To study further the distribution of apoA-I clusters in the LE/LC phase coexistence, we characterized apoA-I cluster distribution in

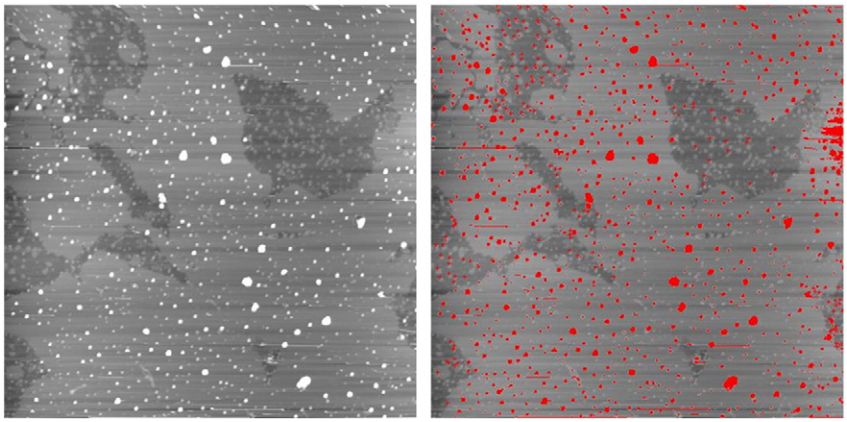

Fig. 3. On the left, AFM images (size: 64 μm^2 and z-range = 10 nm) of mixed monolayers of apoA-II/DPPC, where initial surface pressure was 15 mN/m. On the right, the same image where selected particles in LC phase are colored in red (height above 1.4 nm) and marked by a red cross in LE phase (height adjusted at the height of the LE domain).

DPPG monolayers. The increase of surface pressure produced by the presence of apoA-I at the liquid–DPPG interface is 11 mN/m. Hence, the surface pressure during transference on mica sheet is equal to 26 mN/m. In this case, the lipids have the same acyl chains as DPPC but a different polar headgroup. In the case of DPPC, the polar headgroup is zwitterionic while for DPPG the polar headgroup is anionic. Because in both cases the lipid monolayers show the same phase coexistence, it was possible to test the influence of electrostatic interactions on apoA-I cluster distribution.

ApoA-I/DPPG monolayers show wide bright gray domains that correspond to LC phase and wide dark gray domains that correspond to LE phase (Fig. 1C). As for other apoA-I/phospholipid monolayers, the spotlights correspond to apoA-I clusters. The influence of the LE/LC phase distribution on apoA-I cluster distribution is less important than it is for DPPC as Fig. 1C shows.

Fig. 2 (panel 4) shows the experimental distribution functions of apoA-I clusters derived from AFM images of apoA-I/DPPG monolayers shown in Fig. 1C. The apoA-I cluster distribution was characterized in the entire image and included both phases. Fig. 2 (panel 4) also shows the hard-disk distribution functions for a random distribution of hard-disks in the whole image. Reproducibility was confirmed with three independent AFM images of apoA-I/DPPG monolayers (data not shown). We noted that there is a good agreement between experimental and hard disk distribution functions.

These results revealed that interactions between apoA-I clusters are weak or non-existent in DPPG. Moreover, we noted that the distribution of apoA-I clusters in DPPG is similar to the distribution in DOPC, which is in a single phase, and that it greatly differs from the distribution in DPPC.

3.4. ApoA-II cluster distribution in zwitterionic lipids

Next, we investigated if the phase exerts an important effect on the distribution of protein clusters for an exchangeable apolipoprotein of smaller size than apoA-I. In an attempt to answer this question we studied the distribution of apoA-II clusters in LE/LC phase coexistence of a zwitterionic lipid (DPPC). The increase of surface pressure produced by the presence of apoA-II at the liquid–DPPC interface is 4 mN/m. Hence, the surface pressure during transference on mica sheet is equal to 19 mN/m. AFM images of apoA-II/DPPC monolayers revealed protein clusters that could be seen as spot lights. Wide bright gray domains of AFM images from apoA-II/DPPC layers represent LC phase while wide dark gray domains represent LE phase (Fig. 3). In the case of apoA-II, the protein cluster distribution in DPPC monolayers seems to be homogeneous in spite of the presence of LE/LC coexistence. Fig. 4 shows the apoA-II cluster and hard-disk distribution functions derived from the AFM images of apoA-II/DPPC monolayers presented in Fig. 3. The apoA-II distribution functions were characterized assuming a random distribution of hard disks. Reproducibility was confirmed with five other AFM images (data not shown). The good agreement between the experimental distribution functions and the hard-disk distribution functions indicate a random distribution of apoA-II clusters in a DPPC monolayer.

3.5. Geometrical shape of apoA-I and apoA-II clusters

Using surface pressure measurements and geometrical analysis of protein clusters, we studied the difference between apoA-I and apoA-II interactions with DPPC in an attempt to define why a higher amount of apoA-II than apoA-I interacts with LC phase of DPPC.

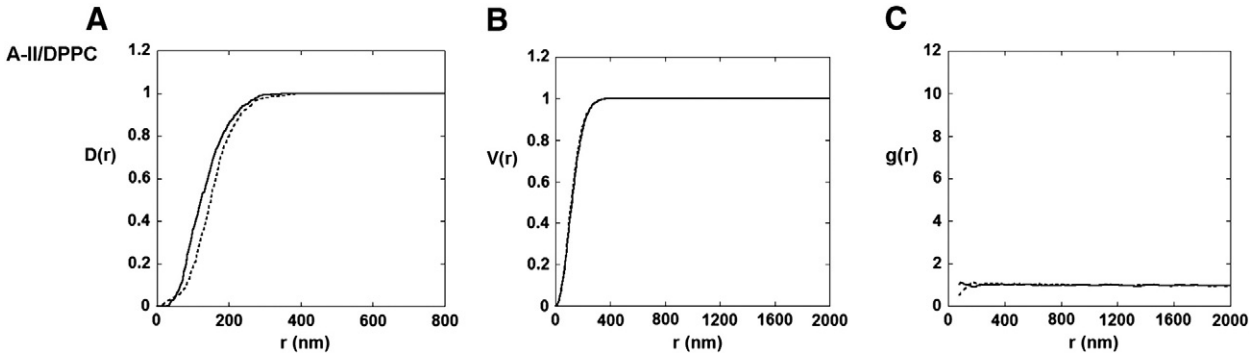

Fig. 4. Analysis of the distribution of protein clusters on AFM-images of apoA-II/DPPC (starting surface pressure 15 mN/m) shown in Fig. 4. D(r) (graph A), V(r) (graph B) and g(r) (graph C) were calculated. The dotted lines show experimental distribution functions of protein clusters, and the thick lines show hard-disk distribution functions.

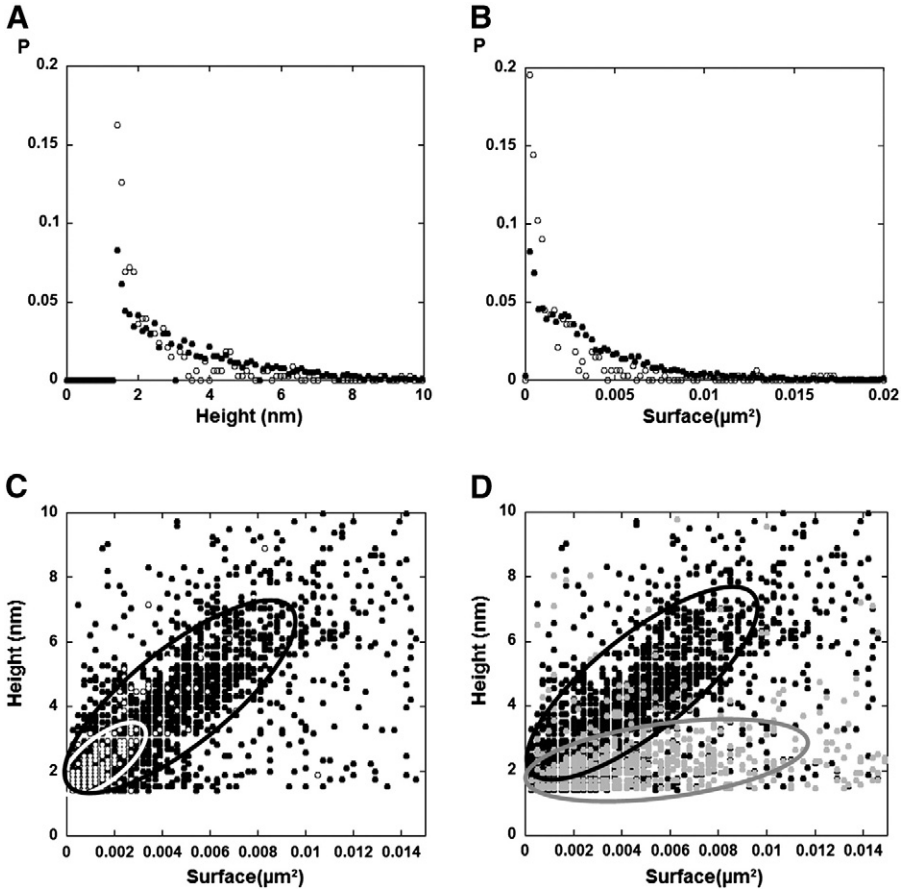

Fig. 5. Normalized histograms of heights (A) and surfaces (B) and graph of height versus surface (C), for protein clusters of apoA-I (○) and apoA-II (●) in LC phase of DPPC at the initial surface pressure of 15 mN/m. Next, graph of height versus surface (D), for apoA-II clusters in LC phase (●) and LE phase (●) of DPPC at the same initial surface pressure.

Surface pressure π was recorded during kinetic of apoA-II adsorption at the liquid/DPPC interface, with $\pi_{initial} = 15$ mN/m. The increase of surface pressure Δπ, which was produced by the presence of apoA-II at the aqueous solution/lipid interface was 4 mN/m. In comparison, the Δπ value produced by apoA-I at the same aqueous solution/lipid interface is the same (4 mN/m) [10]. In both cases, this value is significant and imply the insertion of apoA-I and apoA-II residues in the phospholipid layer [4,26,27].

Fig. 5 shows normalized histograms of height (graph A) and surface (graph B) of apoA-I and apoA-II protein clusters in LC phase of DPPC ($\pi_{initial} = 15$ mN/m). The histograms indicate that objects of greater surface and height are more numerous for apoA-II compared to apoA-I. Hence, objects with surfaces smaller than 0.001 µm² (the pixel size on our AFM images) and heights smaller than 2 nm have a two-fold lower occurrence probability for apoA-II over apoA-I. Moreover, the graph of cluster height versus cluster surface for apoA-I and apoA-II clusters in LC phase of DPPC (Fig. 5C) shows that cluster height increases with cluster surface. From the analysis of this graph it can be noted that the distribution of apoA-II clusters differs from that of apoA-I clusters: apoA-II clusters are higher and wider than the apoA-I ones.

Fig. 5D shows cluster height as a function of cluster surface for apoA-II clusters in DPPC LC and LE phases. The height of objects in LE phase was increased to 1 nm to correct the height difference due to the thickness difference between the two phases. Despite this correction, we noted that objects with identical surfaces are higher in LC phase than in LE phase of the DPPC layer.

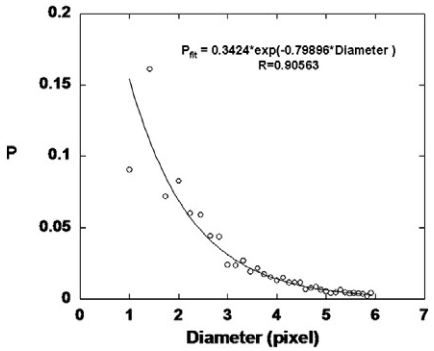

Fig. 6. Normalized histogram of the apoA-I cluster diameter, calculated from six images of DOPC + apoA-I. The diameter distribution used in Monte-Carlo simulations was fitted to this experimental distribution (solid line). The latter was used to simulate the diameter distributions of the three lipids.

3.6. Model for self-assembling of apoA-I and apoA-II clusters

The study of the interaction of apoA-I peptides with lipid bilayers has lead to a cooperative model of peptide aggregation [28]. Such model provides a sound explanation for the decrease in the number of clusters with the diameter (or surface) of apoA-I clusters (Fig. 6) and considers that the initial binding of a protein P to the phospholipid monolayer M occurs as a nucleation step, which is characterized by the equilibrium constant k_1:

$$M + P \underset{}{\overset{k_1}{\rightleftharpoons}} MP \qquad C_{MP} = k_1 \cdot C_L \cdot C_P \tag{1}$$

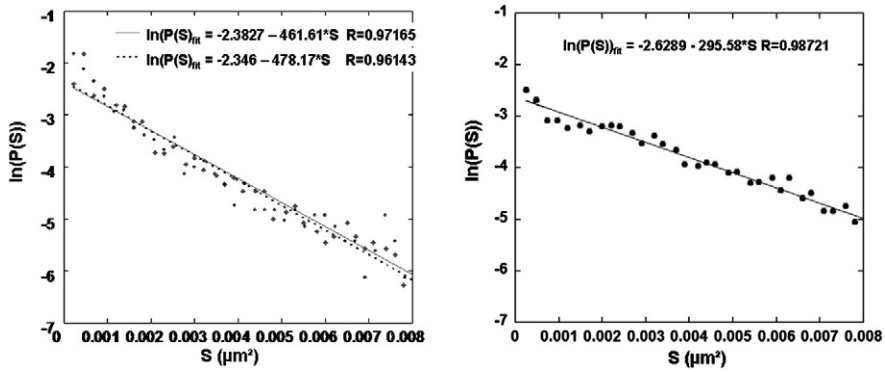

Fig. 7. Logarithm of surface distribution for mixed monolayers, with a starting surface pressure of 15 mN/m. On the left: DOPC + apoA-I (♦) and DPPG + apoA-I (●), on the right: DPPC + apoA-II. These graphs were fitted by Eq. (6), and give values for R that show a good agreement between an auto-assembling model and these distributions. DOPC+apoA-I and DPPC+apoA-II (continous lines), DPPG+apoA-I (dotted line).

where C_L is the lipid concentration, C_P is the protein concentration and C_{MP} is the nucleus concentration.

Further apoA-I binding can be described by growth steps of constant k_2.

Hence, the mechanism for growth step is defined by:

$$MP + P \underset{}{\overset{k_2}{\rightleftharpoons}} MP_2 \qquad C_{MP_2} = k_2 \cdot C_{MP} \cdot C_P = k_2 \cdot k_1 \cdot C_L \cdot C_P^2 \tag{2}$$

$$MP_{n-1} + P \underset{}{\overset{k_2}{\rightleftharpoons}} MP_n \qquad C_{MP_n} = k_2 \cdot C_{MP_{n-1}} \cdot C_P = (k_1/k_2) \cdot C_L \cdot (C_P \cdot k_2)^n. \tag{3}$$

Eq. (3) shows the relation between the concentration of clusters and the number (n) of proteins in the cluster. The surface of the cluster S is related to n and to the surface S_0 occupied by one protein in the lipid monolayer according to the relation: $S = n \cdot S_0$.

Hence, Eq. (3) can be written as a function of the surface S of the cluster, in the following form:

$$C_{MP_n} = (k_1/k_2) \cdot C_L \cdot (C_P \cdot k_2)^{\frac{S}{S_0}}, \qquad S = n \cdot S_0. \tag{4}$$

Now, we can introduce in the previous equation the probability $P(S)$ to find a cluster of a surface S to obtain the new equation:

$$P(S) = A \cdot C_{MP_n} = A \cdot (k_1/k_2) \cdot C_L \cdot (C_P \cdot k_2)^{\frac{S}{S_0}}. \tag{5}$$

Here, A is a constant of normalization. We can simplify Eq. (5) as follows:

$$\begin{aligned} &\ln(P(S)) = \alpha \cdot S + \beta \\ &\text{where} \quad \alpha = \frac{\ln(C_P \cdot k_2)}{S_0} \\ &\text{and} \quad \beta = \ln(A \cdot (k_1/k_2) \cdot C_L) \end{aligned} \tag{6}$$

where $P(S)$ is the value of the normalized histogram for the surface S. The fit of the surface distribution $\ln(P(S))$ by the mathematical model of Eq. (6) is shown in Fig. 7. The value of R is greater than 0.96 for apoA-I/DOPC, apoA-I/DPPG and apoA-II/DPPC. This self-assembling model describes protein cluster formation. It is important to note that the fit of $\ln(P(S))$ could not be performed in the case of apoA-I/DPPC due to the low number of protein clusters in this lipid.

4. Discussion

We have shown that apoA-II is easily inserted in condensed zwitterionic lipid phases while apoA-I is much more sensitive to zwitterionic lipid packing and is rarely found in condensed phase. Both proteins are mainly present as small clusters as revealed by the shape of cluster size histogram on Fig. 5A,B. Furthermore, the lack of repulsion between apolipoprotein clusters indicates that the smallest oligomers of apolipoproteins are not depleted from the lipid layer [29,30]. The presence of these oligomers in the lipid layer reinforces the relevance of our results for the understanding of lipoprotein formation since the newly formed HDL particles contain a small number of apolipoproteins.

Furthermore, our results show that the constant of reaction k_2 of apoA-II with zwitterionic lipids, obtained from a simple self-assembling model is higher than that of apoA-I, although the geometrical shape of the clusters formed by these proteins is similar (that point is detailed in the Supplementary material section). Hence, we conclude that the self-assembling rate of apoA-I is rather unfavorable and cannot explain the faster lipoprotein formation rate of apoA-I in comparison to apoA-II.

Now, the interaction of apoA-I and apoA-II α-helices with zwitterionic phospholipid is in both cases governed mainly by hydrophobic effect due to the absence of net charge of the lipid polar head-group. Moreover, apoA-I sensitivity to lipid packing is negligible when strong electrostatic interactions are present as proved by the random repartition of apoA-I in the anionic phospholipid DPPG (Figs. 1C and 2 panel 4). Finally, we attribute the higher sensitivity of apoA-I to lipid packing as due to the higher number of amphipathic α-helix repeats compared to apoA-II since apoA-I contains eight 22-mer and two 11-mer class A amphipathic α-helices while apoA-II only contains three 11-mer of such amphipathic α-helices [1].

Moreover, sensitivity to lipid packing modulated by a relatively balanced set of electrostatic and hydrophobic interactions has been described for the Golgi-associated protein ArfGAP1 containing the amphipathic lipid packing sensor (ALPS) motif [31]. The latter is organized as an α-helix repeat which is characterized by a polar face rich in non-charged (threonine and serine) amino acid residues. To insert into the membrane, ALPS α-helix repeat motif undergoes a disorder-to-order conformational transition to overcome an energy barrier. ALPS membrane insertion is not highly energetically favorable due to the absence of electrostatic interactions and is prevented by a high lipid packing in the membrane. Drin and Antonny have compared the curvature sensitivity between native ArfGAP1 and a mutant form of similar charged residue distribution as class A2 amphipathic α-helix repeat motifs of exchangeable apolipoproteins [32]. They presented evidence of sensitivity to curvature for ArfGAP1 in the presence of an anionic lipid (PS) where hydrophobic effects were dominant for the native protein. They also showed that that was not the case of the ArfGAP1 mutant where electrostatic and hydrophobic effects were more balanced. Interestingly, native and mutant ArfGAP1 exhibited sensitivity to curvature in the presence of zwitterionic lipids where electrostatic interactions with lipid head-group are weak or absent. These results showed that the different distributions of amino acid residues of class A1 and class A2 amphipathic α-helices were not responsible for the

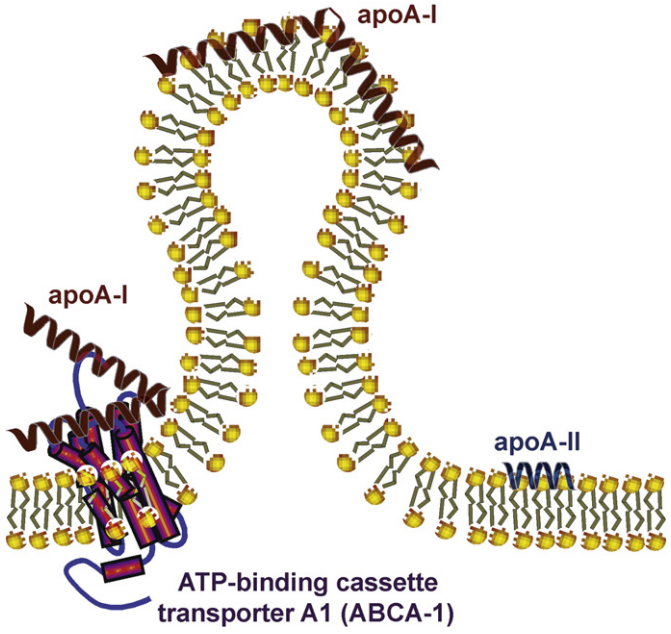

Fig. 8. Model of preferential binding of apoA-I in highly curved protrusions. ApoA-I inserts preferentially in the external vesiculated protrusions induced by phospholipid translocation due to the low lipid packing of these protrusions. The subsequent lipid solubilization would lead to the formation of apoA-I-containing nascent discoidal HDL particles. By contrast, apoA-II would insert randomly in the external leaflet and therefore show a lower probability to form nascent discoidal HDL.

different sensitivities to the packing of zwitterionic lipids. Furthermore, the increase of lipid packing sensitivity with the number of α-helix repeats and a "Velcro" model in which the insertion of a protein into the membrane requires a disorder-to-order conformational change of ALPS motifs has been suggested by others [33]. The insertion becomes more unfavorable and the binding probability decreases when the number of ALPS motifs in the protein structure increases.

Here, we show that apolipoprotein sensitivity to zwitterionic lipid packing exhibit features that resemble ALPS lipid sensitivity in relation to membrane curvature. Indeed, in our experiments the modulation of the surface of a Langmuir trough reproduces the change of lipid packing of the polar headgroup encountered when membrane curvature changes. Furthermore, a sensitivity of exchangeable apolipoprotein insertion relative to vesicle curvature has been suggested in early interfacial studies of apoA-I and more recently, apolipophorin III [34,35]. We therefore suggest that the mechanistic Velcro model initially proposed to describe ALPS sensitivity to lipid packing is also valid for exchangeable apolipoproteins apoA-I and apoA-II and possibly other lipid binding proteins such as CETP (cholesterol ester binding protein) [8].

The difference in lipid packing sensitivity between proteins of the same family sharing high structure similarity shed some light into the distinctive biological functions of apoA-I and apoA-II. We provide evidence that the preferential insertion of apoA-I near protrusions following ABCA1 activation [9,11] is due to the low lipid packing of the protrusions. The subsequent lipid solubilization would lead to the formation of apoA-I-containing nascent discoidal HDL particles. By contrast, apoA-II would insert randomly in the external leaflet and therefore show a lower probability to form nascent discoidal HDL, thus explaining the well established low proportion of apoA-II in discoidal HDL particles [12,13]. The graphic model presented in Fig. 8 shows the molecular difference in the mechanism of interaction of these proteins with lipid layers.

This idea is strongly supported by a recent study of apoA-I mimetic peptides [17] where cholesterol efflux from cells in the presence of two peptides, 4F and mFc-2X4F (a peptide generated by fusing two 4F peptides with the Fc fragment of mouse IgG) was compared. The authors of that study went further and showed that although the maximum efficiency of cholesterol efflux is the same for both peptides, the concentration of peptides required to reach 50% of the maximum efficiency (EC50) is clearly different. Indeed the EC50 value of the longer peptide is three times lower than the EC50 value of the other one. This result reinforces the hypothesis of a higher HDL formation rate caused by the gathering of apoA-I into protrusions and that such gathering is caused by the larger number of helical repeats in the apoA-I structure when compared to apoA-II.

Taken together, our studies allow us to attribute the higher lipid packing sensitivity of apoA-I relative to zwitterionic lipids to a higher number of amphipathic α-helix repeats compared to apoA-II. Furthermore, considering that anionic lipids are scarce in the external leaflet of the plasma membrane, we postulate that lipid packing sensitivity plays a major role in the interaction of apolipoproteins with the biological membrane.

5. Conclusions

The sensitivity to lipid packing opens the possibility to modulate the interaction of a protein with a lipidic membrane by interfering with the number of amphipathic α-helix tandem repeat motifs and/or the extent of hydrophobic versus polar interactions [32,33,36]. We have shown that apoA-I and apoA-II, two prominent members of the family of exchangeable apolipoproteins that share an important secondary structure feature do not have the same sensitivity to lipid packing. The higher number of class A amphipathic α-helix tandem repeat motifs in apoA-I should account for its relative sensitivity to lipid packing in conditions where electrostatic interactions are negligible (for example, in the presence of zwitterionic lipids) and does not show such sensitivity in the presence of anionic lipids. Furthermore, the comparatively smaller exchangeable apolipoprotein apoA-II is not sensitive to lipid packing even in the presence of a zwitterionic lipid. As HDL particles are produced from highly curved domains of the cell membrane, we postulate that a different lipid packing affinity has evolved as a selection mechanism for HDL production by apoA-I over apoA-II.

Acknowledgement

This work was supported by grants from "Région Bretagne".

Appendix A. Supplementary data

Supplementary data to this article can be found online at http://dx.doi.org/10.1016/j.bbamem.2012.05.016.

References

[1] J.P. Segrest, M.K. Jones, H. De Loof, C.G. Brouillette, Y.V. Venkatachalapathi, G.M. Anantharamaiah, The amphipathic helix in the exchangeable apolipoproteins: a review of secondary structure and function, J. Lipid Res. 33 (1992) 141–166.
[2] V.M. Bolanos-Garcia, S. Ramos, R. Castillo, J. Xicohtencatl-Cortes, J. Mas-Oliva, Monolayers of apolipoproteins at the air/water interface, J. Phys. Chem. B 105 (2001) 5757–5765.
[3] V.M. Bolanos-Garcia, A. Renault, S. Beaufils, Surface rheology and adsorption kinetics reveal the relative amphiphilicity, interfacial activity, and stability of human exchangeable apolipoproteins, Biophys. J. 94 (2008) 1735–1745.
[4] J.A. Ibdah, K.E. Krebs, M.C. Phillips, The surface properties of apolipoproteins A-I and A-II at the lipid/water interface, Biochim. Biophys. Acta, Lipids Lipid Metab. 1004 (1989) 300–308.
[5] H. Saito, P. Dhanasekaran, D. Nguyen, E. Deridder, P. Holvoet, S. Lund-Katz, M.C. Phillips, Alpha-helix formation is required for high affinity binding of human apolipoprotein A-I to lipids, J. Biol. Chem. 279 (2004) 20974–20981.
[6] B.W. Shen, A.M. Scanu, Properties of human apolipoprotein A-I at the air–water interface, Biochemistry 19 (1980) 3643–3650.
[7] P.J. Barter, Hugh Sinclair lecture: the regulation and remodelling of HDL by plasma factors, Atheroscler. Suppl. 3 (2002) 39–47.

[8] V.M. Bolanos-Garcia, M. Soriano-Garcia, J. Mas-Oliva, CETP and exchangeable apoproteins: common features in lipid binding activity, Mol. Cell. Biochem. 175 (1997) 1–10.
[9] O. Chambenoit, Y. Hamon, D. Marguet, H. Rigneault, M. Rosseneu, G. Chimini, Specific docking of apolipoprotein A-I at the cell surface requires a functional ABCA1 transporter, J. Biol. Chem. 276 (2001) 9955–9960.
[10] L. Chièze, V.M. Bolanos-Garcia, M. Pinot, B. Desbat, A. Renault, S. Beaufils, V. Vié, Fluid and condensed ApoA-I/phospholipid monolayers provide insights into ApoA-I membrane insertion, J. Mol. Biol. 410 (2011) 60–76.
[11] C. Vedhachalam, P.T. Duong, M. Nickel, D. Nguyen, P. Dhanasekaran, H. Saito, G.H. Rothblat, S. Lund-Katz, M.C. Phillips, Mechanism of ATP-binding cassette transporter A1-mediated cellular lipid efflux to apolipoprotein A-I and formation of high density lipoprotein particles, J. Biol. Chem. 282 (2007) 25123–25130.
[12] C.C. Hedrick, A.J. Lusis, Apolipoprotein A-II: a protein in search of a function, Can. J. Cardiol. 10 (1994) 453–459.
[13] M.M. Hussain, V.I. Zannis, Intracellular modification of human apolipoprotein AII (apoAII) and sites of apoAII mRNA synthesis: comparison of apoAII with apoCII and apoCIII isoproteins, Biochemistry 29 (1990) 209–217.
[14] A.M. Scanu, C. Edelstein, HDL: bridging past and present with a look at the future, FASEB J. 22 (2008) 4044–4054.
[15] C. Vedhachalam, P.S. Chetty, M. Nickel, P. Dhanasekaran, S. Lund-Katz, G.H. Rothblat, M.C. Phillips, Influence of apolipoprotein (Apo) A-I structure on nascent high density lipoprotein (HDL) particle size distribution, J. Biol. Chem. 285 (2010) 31965–31973.
[16] C. Vedhachalam, A.B. Ghering, W.S. Davidson, S. Lund-Katz, G.H. Rothblat, M.C. Phillips, ABCA1-induced cell surface binding sites for ApoA-I, Arterioscler. Thromb. Vasc. Biol. 27 (2007) 1603–1609.
[17] S.-C. Lu, L. Atangan, K.W. Kim, M.M. Chen, R. Komorowski, C. Chu, J. Han, S. Hu, W. Gu, M. Veniant, M. Wang, An apoA-I mimetic peptibody generates HDL-like particles and increases alpha-1 HDL subfraction in mice, J. Lipid Res. 53 (2012) 643–652.
[18] G.D. Wool, C.A. Reardon, G.S. Getz, Apolipoprotein A-I mimetic peptide helix number and helix linker influence potentially anti-atherogenic properties, J. Lipid Res. 49 (2008) 1268–1283.
[19] P.G. Yancey, J.K. Bielicki, W.J. Johnson, S. Lund-Katz, M.N. Palgunachari, G.M. Anantharamaiah, J.P. Segrest, M.C. Phillips, G.H. Rothblat, Efflux of cellular cholesterol and phospholipid to lipid-free apolipoproteins and class A amphipathic peptides, Biochemistry 34 (1995) 7955–7965.
[20] C.W. Hollars, R.C. Dunn, Submicron structure in L-adipalmitoylphosphatidylcholine monolayers and bilayers probed with confocal, atomic force, and near-field microscopy, Biophys. J. 75 (1998) 342–353.
[21] V. Vie, N. Van Mau, L. Chaloin, E. Lesniewska, C. Le Grimellec, F. Heitz, Detection of peptide–lipid interactions in mixed monolayers, using isotherms, atomic force microscopy, and Fourier transform infrared analyses, Biophys. J. 78 (2000) 846–856.
[22] V. Vié, S. Legardinier, L. Chieze, O. Le Bihan, Y. Qin, J. Sarkis, J.F. Hubert, A. Renault, B. Desbat, E. Le Rumeur, Specific anchoring modes of two distinct dystrophin rod sub-domains interacting in phospholipid Langmuir films studied by atomic force microscopy and PM-IRRAS, Biochim. Biophys. Acta, Biomembr. 1798 (2010) 1503–1511.
[23] C. Bottier, J. Géan, B. Desbat, A. Renault, D. Marion, V. Vié, Structure and orientation of puroindolines into wheat galactolipid monolayers, Langmuir 24 (2008) 10901–10909.
[24] O. Albrecht, H. Gruler, E. Sackmann, Polymorphism of phospholipid monolayers, J. Phys. Fr. 39 (1978) 301–313.
[25] L. Tamm, H.M. McConnel, Supported phospholipid bilayers, Biophys. J. 47 (1985) 105–113.
[26] J.A. Ibdah, S. Lund-Katz, M.C. Phillips, Molecular packing of high-density and low-density lipoprotein surface lipids and apolipoprotein A-1 binding, Biochemistry 28 (1989) 1126–1133.
[27] J.A. Ibdah, M.C. Phillips, Effects of lipid composition and packing on the adsorption of apolipoprotein A-I to lipid monolayers, Biochemistry 27 (1988) 7155–7162.
[28] P. Spuhler, G.M. Anantharamaiah, J.P. Segrest, J. Seelig, Binding of apolipoprotein A-I model peptides to lipid bilayers. Measurement of binding isotherms and peptide–lipid headgroup interactions, J. Biol. Chem. 269 (1994) 23904–23910.
[29] U. Bernchou, J.H. Ipsen, A.C. Simonsen, Growth of solid domains in model membranes: quantitative image analysis reveals a strong correlation between domain shape and spatial position, J. Phys. Chem. 113 (2009) 7170–7177.
[30] M. Losche, H.P. Duwe, H. Möhwald, Quantitative analysis of surface textures in phospholipid monolayer phase transitions, J. Colloid Interface Sci. 126 (1988) 432–444.
[31] J. Bigay, J.F. Casella, G. Drin, B. Mesmin, B. Antonny, ArfGAP1 responds to membrane curvature through the folding of a lipid packing sensor motif, EMBO J. 24 (2005) 2244–2253.
[32] G. Drin, J.F. Casella, R. Gautier, T. Boehmer, T.U. Schwartz, B. Antonny, A general amphipathic alpha-helical motif for sensing membrane curvature, Nat. Struct. Mol. Biol. 14 (2007) 138–146.
[33] B. Antonny, Mechanisms of membrane curvature sensing, Annu. Rev. Biochem. 80 (2011) 101–123.
[34] C.-P.L. Wan, M.H. Chiu, X. Wu, S.K. Lee, E.J. Prenner, P.M.M. Weers, Apolipoprotein-induced conversion of phosphatidylcholine bilayer vesicles into nanodisks, Biochim. Biophys. Acta, Biomembr. 1808 (2011) 606–613.
[35] J.R. Wetterau, A. Jonas, Effect of dipalmitoylphosphatidylcholine vesicle curvature on the reaction with human apolipoprotein A-I, J. Biol. Chem. 257 (1982) 10961–10966.
[36] G. Drin, B. Antonny, Amphipathic helices and membrane curvature, FEBS Lett. 584 (2010) 1840–1847.